Photochemistry and Photobiology, 2013, 89: 1346–1353

Modulation of the Photophysical Properties of Pyrene by the Microstructures of Five Poly(alkyl methacrylate)s Over a Broad Temperature Range†

Teresa D. Z. Atvars[1], Shibu Abraham[2§], Anita J. Hill[3,4], Steven J. Pas[3,4], Carlos Chesta[5] and Richard G. Weiss[2*]

[1]Chemistry Institute, State University of Campinas (Unicamp), Campinas, Brazil
[2]Department of Chemistry and Institute for Soft Matter Synthesis and Metrology, Georgetown University, Washington, DC
[3]CSIRO Materials Science and Engineering and Process Science and Engineering, South Clayton, Vic., Australia
[4]Monash University, Department of Materials Engineering and Chemistry, Clayton, Vic., Australia
[5]Departamento de Química, Universidad Nacional de Río Cuarto, Río Cuarto, Argentina

Received 11 March 2013, accepted 21 May 2013, DOI: 10.1111/php.12103

ABSTRACT

Pyrene fluorescence spectra have been recorded in five poly (alkyl methacrylate)s (where alkyl is ethyl butyl, isobutyl, cyclohexyl and hexadecyl) over a 20–400 K temperature range. The changes in the position and the full width at half maximum (FWHM) of the 0–0 emission band (peak I) have been correlated with the structural characteristics of the alkyl groups in the different relaxation regimes of the polymers to assess the degree of coupling of the excited singlet states with the polymer cybotactic regions. Data treatment of the peak I positions using an electron–phonon model indicates that longitudinal optical modes are involved, and that the magnitude of coupling depends on the polymer structure and follows the same trend as the glass transition temperatures. The same spectral parameters have been correlated also with "hole" free volumes from positron annihilation spectroscopy over temperature ranges which span the glass or melting transitions of the polymers. Reasons why free volume and FWHM measurements follow the same trends, and other aspects of the systems, are discussed.

INTRODUCTION

Acrylic polymers form a class of materials whose bulk properties depend strongly on their structures, especially their type of lateral chain (1–3). In particular, one important factor determining the properties of poly(alkyl methacrylate)s (PAMAs) is the type (size and branch lengths) of the alkyl groups attached to the carboxyl moieties. PAMAs with short alkyl or branch groups provide amorphous materials; those with longer *n*-alkyl chains (*i.e.* 12 or more carbon atoms) form semicrystalline domains at ambient temperatures (4). Various diffraction and scattering techniques are able to interrogate intimate structural aspects of chain packing. For example, evidence of local order in the amorphous phases of polymers has been demonstrated by wide angle X-ray scattering (5). In some PAMAs, the local structure consists of layers of the rigid, more polar backbone separated by the more flexible and less polar alkyl branches which, themselves, have varying degrees of order. As a consequence of these structural properties, PAMAs generally exhibit complex morphologies and very microheterogeneous matrixes.

Molecular probes are widely used now to sense microenvironments (*i.e.* the cybotactic[1] regions composed of the chains in the immediate vicinity of the probe) in polymer systems. In particular, there are probes for sensing polarity, microviscosity, the presence of impurities, polymer relaxation processes, selectivity in chemical reactions, *etc*. (6–17). Positron annihilation spectroscopy is a probe of "hole" free volumes (18,19). It relies on analyses of the decay profiles of positroniums, which are created in all the regions of a polymer matrix when a positron from an external source (usually, the decay of ^{22}Na) combines with an electron of the polymer. The data from such measurements are very useful in assessing the distribution and the sizes of hole types in the absence of a probe molecule. As any probe molecule must disturb its local environment to some extent, the ability to assess the free volume in "pristine" polymers affords valuable information about how and which sizes of guest molecules might be accommodated easily within a polymer matrix. Data of this type have been used by others and us to correlate both photochemical and photophysical properties of guest molecules in several polymers (9,13,20).

Photoluminescence from probe molecules has been found to be a very useful and more general technique to investigate structural and dynamic aspects of polymer morphology at the subnanometer scale. Depending on the type of emission property being measured (*e.g.* spectral shape and position, lifetime, anisotropy,

*Corresponding author email: weissr@georgetown.edu (Richard G. Weiss)
†This article is part of the Special Issue dedicated to the memory of Elsa Abuin.
§Current address: SBG Labs, Inc., Sunnyvale, CA.

[1]"That part of a solution in the vicinity of a solute molecule in which the ordering of the solvent molecules is modified by the presence of the solute molecule." IUPAC Compendium of Chemical Terminology, 2nd ed. (the "Gold Book"). Compiled by A. D. McNaught and A. Wilkinson. Blackwell Scientific Publications, Oxford (1997).

band width, hole burning, *etc.*), different correlations with an aspect of the polymer matrix can be observed (7,11).

For example, a purely electronic 0–0 transition (*i.e.* from the lowest vibronic level of the initial state to the lowest vibronic level of the final state) of a guest in a matrix, whether it be a liquid, crystal, polymer, inorganic cavity, *etc.*, may undergo spectral broadening (8,10,21–23). The nature of the broadening depends on the type and intimacy of the host–guest interactions, on the guest mobility within its cybotactic region, and on temperature (24–34). Generally, two parameters contribute to spectral broadening:

1. "Inhomogeneous" broadening arises from the slightly different cybotactic regions experienced by molecules of the same structure dispersed in a matrix (6,22). The individual spectra of the molecules may differ somewhat due to the distribution of environments offered by the cybotactic regions, and the observed emission spectrum from the ensemble is a convolution of the contributions from molecules in each site type weighted by their relative populations; the more disordered the system is, the more varied will be the range of the cybotactic regions and the broader will be the spectrum of the probe.
2. In the absence of energy transfer processes, a "homogeneous" contribution to spectral broadening results from relaxation of the population of excited-state molecules. It depends on the lifetimes of the excited states, spectral diffusion and the rates of conformational or rotational relaxation processes (6,26,29–33, 35–37). Homogeneous relaxation is very common for guest molecules in solid matrixes at lower temperatures, principally when excitation leads to large changes in charge distribution or molecular shape. It is also important in attached pigments bound to disordered, glass-like proteins (22,24,26–28,32,37).

For aromatic organic molecules in a solid matrix, the relative contribution of homogeneous broadening is usually smaller than that of inhomogeneous broadening. Molecules sorbed in a polymer or in a frozen solution commonly show inhomogeneous broadening of ~300 cm^{-1}, ~1–10 cm^{-1} in a solid crystal and only ~0.03 cm^{-1} in a single crystal (37). Inhomogeneous broadening is also more important than homogeneous broadening in solids at low temperatures (7,31,32). Additional homogeneous broadening occurs as a result of contributions associated with the lifetime of the excited state (population relaxation), from the dephasing rate (caused by thermal fluctuations of the environment), and from orientational relaxation processes leading to loss of correlation of the ensemble of transition dipoles (22,25,27,29,33).

Each of these has a different dependence on temperature (31,38–41). The inhomogeneous broadening is only slightly dependent on temperature if the configurational interactions between the guest molecules and the cybotactic regions of the host matrix do not change over periods which are "long" with respect to the excited-state lifetimes. The smaller is the inhomogeneity, the smaller will be the spectral full width at half maximum (FWHM, Γ). This static behavior is often observed at low temperatures where the structure is frozen and, in general, this is the more important contribution to the spectral broadening. For organic molecules, it can be on the order of hundreds of wavenumbers.

The other processes contributing to line broadening are dynamic and are related to fluctuations of the microenvironments, such as dephasing and orientational relaxations; they are attenuated strongly at very low temperatures. Thus, excited-state lifetimes become a dominant factor under this condition (23,24,27,29–31,33,40). At higher temperatures, dephasing is a major contributor to homogeneous broadening (27,33,36). Several reports document the extent of the increases in homogeneous broadening with temperature. It is dependent on the strength of the coupling between the molecular transition dipole of the guest molecule and the thermal bath afforded by the host polymer matrix (31,38–41). Monotonic increases of homogeneous broadening have been reported over ranges of increasing temperature (24,29,31,32,39–41) that do not include a phase transition of the host matrix.

A rapid increase in dephasing of guest molecules is observed in materials being heated through the onset of a thermal relaxation process, such as a glass transition (T_g), which can lead to changes in the inhomogeneous broadening as well as result in the freeing of longer chain segment motions in the polymer. The specific form of the dependence of homogeneous broadening on temperature is different for the glass transition in each polymer. At lower temperatures, the effective homogeneous broadening in glasses follows a power law dependence (Eq. 1):

$$\Gamma(T) = \Gamma_0 + AT^{\alpha} \tag{1}$$

where $1 \leq \alpha \leq 2$, has been found for optical dephasing in a variety of glasses (25,26,31,33,35). This power law is similar to the temperature dependence of the heat capacity (25). The rapid increase above T_g is due to thermally activated spectral dephasing. For several organic glasses and polymers, the temperature dependence of the homogeneous broadening caused by spectral diffusion follows a power law with $T^{1.3}$ at temperatures below 20 K, independent of the guest and the host (36).

In summary, two classes of spectral broadening operate in polymer matrixes: one is provided by the static, heterogeneous distribution of the cybotactic layer of chains around each guest molecule; the other arises from fluctuations of the cybotactic layer during the excited-state lifetime of the guest and from the structural relaxation of the solvent. When the time resolution of an experiment is faster than the lifetime of the emitting state of a guest molecule, the spectral diffusion that produces the spectral broadening can be deciphered (22,23,27–30,42).

Other spectral parameters that are temperature dependent are the peak positions of the absorption and the emission bands (38,43). The temperature dependence of the band position of the photoluminescence spectrum may be blue or red shifted as a consequence of a redistribution of the exciton energies by electron–phonon interactions which activate lower energy acoustical and optical phonons (32,37–40,43). For inorganic semiconductors, the band gap energy decreases with the temperature according to the Bose–Einstein statistical factor for phonon emission plus absorption (Eq. 2) (32,37–42). For inorganic materials, two mechanisms are involved with the temperature dependence of the line shift at constant pressure: the thermal expansion and the electron–phonon interaction that removes the excited-state energy (37–42). The latter is usually more important. This model has been applied successfully to organic materials, as well, including aromatic molecules, conjugated oligomers and conjugated polymers (37–42).

$$E_{00}(T) - E_{00}(T = 0\,\mathrm{K}) = -\frac{2a}{\exp(\theta/T) - 1} \tag{2}$$

where E_{00} (T = 0 K) is the energy gap at 0 K, θ is the average phonon temperature and a is the electron–phonon interaction (33,38,39). Parameter a contains the contribution of both the

acoustic and the optical phonons (31,39). Higher values of θ indicate that the optical phonons are playing a greater role on electron–phonon coupling compared with acoustic phonons. The optical phonons are due to the carbon–carbon stretching modes for aromatic organic molecules (longitudinal modes) or bending and torsional motions (transverse modes) (31,39). For example, the average $a = 0.065 \pm 0.01$ eV in *para*-hexaphenyl, with an average $\theta = 530 \pm 150$ K, whereas for GaAs, the values are $a = 0.057$ eV and $\theta = 240$ K (31,39).

Previously, we studied polymer relaxation processes using the intensities of unimolecular excited state and intermolecular excimer emissions from pyrene as a guest in some PAMAs ((poly (ethyl methacrylate) (PEMA), poly(*n*-butyl methacrylate) (PBMA), (poly(isobutyl methacrylate) (PIBMA), poly(cyclohexyl methacrylate) (PCHMA) and (poly(*n*-hexadecyl methacrylate) (PHDMA)) in the temperature range from 20 to 410 K (Table 1) (17). In that work, we also examined the dependence of the intramolecular exciplex emissions from *N,N*-dimethyl-3-(pyren-1-yl) propan-1-amine as a function of PAMA type and temperature. The dynamics of the excimer and exciplex emissions were found to be influenced by polymer structure: in matrixes of PEMA and PBMA, PAMAs with short alkyl groups capable of occupying small cross-sectional areas near the main chain, excited state complex formation was less efficient than in the other PAMAs due to the ability of the guests to reside in cybotactic regions closer to the main chain and, thus, to adopt more elongated conformations (*i.e.* reducing guest mobility). In matrixes of PIBMA and PCHMA, with more rigid and branched alkyl groups, guest molecules appear to reside on average in cybotactic regions which are farther from the main chain and are less restricted to undergo conformational changes. In PHDMA, below its melting temperature, the guest molecules are excluded from the crystalline regions of the long alkyl side chains, and only shorter range mobility of the guests is thought to be allowed; the alkyl segments near the main chain which are not crystalline are much less free than those of PEMA and PBMA, where no side group crystallization occurs.

In general, the density of a polymer matrix is anisotropic at the micrometer distance scale; higher and lower density regions exist especially in amorphous regions. In the crystalline domains of semicrystalline polymers, density gradients may exist as well. The regions of greatest interest to imbibing guest molecules have lower densities with "hole" whose free volumes may be measured using positron annihilation techniques (44,45). Somewhat surprisingly, the nature of the photochemical and photophysical processes of a set of probe molecules, did not appear to depend acutely on hole free volume (13) although they do in polyethylene matrixes (13,46,47).

Table 1. T_g (or T_m for PHDMA) of the PAMAs and the temperature of the polymer relaxation processes determined by the emission intensity in Ref. (18).

PAMA	T_g/K	T_γ†	T_β†	T_α†	Γ_{inh}/cm^{-1} (T = 0 K)
PCHMA	368	160	260	330	215 ± 7
PEMA	342	159	269	322	235 ± 6
PIBMA	322	140	210–240	330	307 ± 6
PBMA	299	150	240	290	251 ± 5
PHDMA	281*	130	220	280	350 ± 6

*T_m; †data from Ref. (18); other values obtained in the literature (2,3,23,50,51) (are in the same range).

Assuming that each PAMA matrix has a somewhat different solvating ability around pyrenyl groups (*i.e.* each submits the pyrene molecules to a different set of cybotactic regions), different contributions of the heterogeneous and homogeneous broadening to the spectral width might occur, with the more ordered matrixes producing smaller heterogeneous broadening. For example, the spectral properties of a dye are known to depend on the size and shape of its cavity in hydrocarbon solvents. If the solvent and dye are similar in size, narrower line widths in the spectra might be expected (48). However, no attempt to correlate spectral broadening from pyrene fluorescence and hole free volume in the PAMAs has been made. Thus, their potential contribution to the appearance of the emission from pyrene molecules within the PAMA matrixes is unknown. For that reason and because this information is relevant to the interactions of many other probes in a wide range of polymers, here we have investigated possible relationships between line broadening of the fluorescence from pyrene guest molecules and both the order and hole free volumes of the matrixes of the PAMAs. Among the treatments employed are the usual power law models for the dependence of spectral broadening on temperature. However, they are extended to consider other spectroscopic parameters, the FWHM and wavelength shift of the 0–0 emission band. FWHM provides information about the distribution of the cybotactic sites afforded to the pyrene guests and their host–guest interactions; the peak position of the 0–0 band yields information about the efficiency of the electron–phonon coupling and the mechanism of the coupling with either acoustic or longitudinal vibrational modes.

MATERIALS AND METHODS

Materials and sample preparations. PEMA, PBMA, PCHMA and PHDMA were purchased from Scientific Polymer Products, Inc. PIBMA was obtained from Aldrich. They were purified as described in Ref. (16) and some of their physical properties of these polymers are collected in Table 1. Pyrene (PyH) (Aldrich, 99%) was recrystallized twice from ethanol.

Films of the PAMAs, doped with pyrene (PyH), were prepared by casting dichloromethane or chloroform solutions containing 10^{-4} mol PyH/kg polymer onto Teflon plates. After solvent evaporation at room temperature in a dry atmosphere, the films (except PHDMA) were heated to above their glass transition temperatures and then cooled to room temperature. Finally, the samples were kept in a desiccator at 0.2 Torr under dynamical vacuum for 6–12 h and static vacuum for 12–24 h. The samples were flamed sealed in degassed <10–5 Torr, flattened pyrex capillaries.

Instrumentation. Fluorescence measurements of PyH in the PAMAs were carried out at 20–420 K at increments of 10°C within a closed He-cycle cryosystem from APD Cryogenics, using a SPEX 0.5 m spectrograph. Excitation was with the 325 nm line of a Kimmon model IK helium–cadmium laser.

Data treatment. At each temperature, the FWHM (in cm^{-1}) and the wavelength maximum of the 0–0 emission band (peak I) of pyrene was deconvoluted from the rest of the emission spectrum using a Gaussian function using Origin-8 software. The FWHM of peak I was calculated by deconvoluting it from contributions from neighboring bands in the 26 650–27 100 cm^{-1} wavenumber interval (chosen by the best fit of the emission spectrum at 20 K in each PAMA). This procedure gave the peak position, $E_{00}(T)$, as well. The band width at $T \rightarrow 0$ K, obtained by extrapolation was calculated for each of the PAMAs and used to calculate the broadening, $\frac{\Gamma(T)-\Gamma(T=0\,K)}{\Gamma(T_g)-\Gamma(T=0\,K)}$. These values were plotted *versus* reduced temperature, T/T_g or T/T_m. The experimental data for the redline shift with temperature were simulated by Eq. (2) using MatLab software to fit the experimental data.

Methods for calculating the hole free volumes of the PAMAs over the temperature range explored are described in detail in Ref. (13). Basically,

temporal decay profiles of the positrons (emitted from a sealed ^{22}Na source sandwiched between PAMA films under a nitrogen atmosphere) were fitted to three time constants using the LT9 software (49). Averages of the long lifetime component, attributed to ortho-positroniums localized in free volumes, were obtained from three repeat experiments and were used to calculate the free volumes reported.

RESULTS AND DISCUSSION

Figure 1 shows one example of the temperature dependence of the photoluminescence spectra of pyrene as a guest in PCHMA. The luminescence spectra of pyrene in the other PAMAs are shown in Figure S1.

Plots of the FWHM [$\Gamma(T)$] *versus* temperature for peak I of pyrene emissions in all the PAMAs employed are shown in Fig. 2. Peak I was selected for analysis because it is thought to represent the 0–0 emission band from the first excited singlet state and it is sensitive to several types of perturbations. Experiments to determine the temperature dependence of the emission spectra in two of the PAMAs, PBMA and PCHMA, were repeated to assess the degree of reproducibility (Figures S2 and S3). Although the absolute intensities of the data varied somewhat between runs (due to small variations in film thickness and contour), the FWHM values and the relative intensity changes with temperature were virtually the same. Thus, data treatments reported here involve one run only.

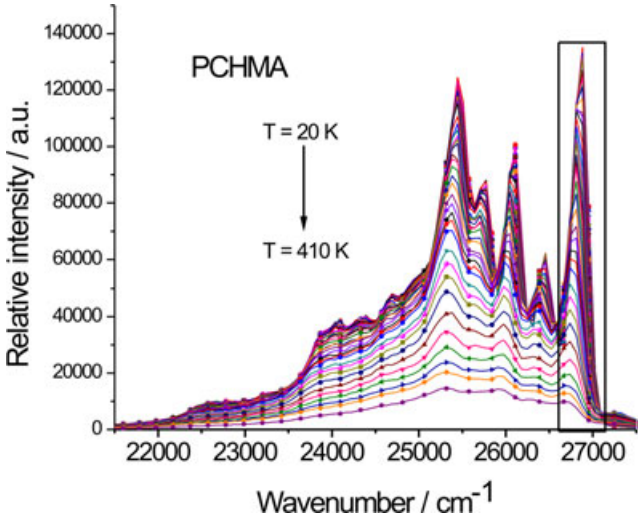

Figure 1. Temperature dependence of the photoluminescence spectrum of pyrene dispersed in PCHMA (λ_{ex} = 325 nm). The rectangle indicates peak I (centered near 370 nm) used for the FWHM and peak position determinations.

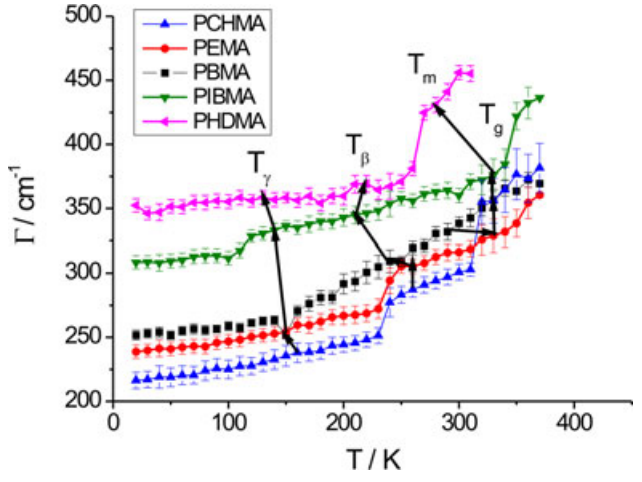

Figure 2. Spectral broadening of the peak I (λ_{em} = 373–375 nm) pyrene fluorescence in the PAMA films as a function of temperature. Arrows indicate the onsets of the relaxation temperatures determined from emission spectra as described in Ref. (16). The error bars are based upon the differences between the average values for two separate runs on two different samples.

As expected, the FWHM is only weakly temperature dependent at lower temperatures. The FWHM increases more acutely as the temperature is raised further, and it experiences discontinuities at specific temperatures. The FWHM value extrapolated to 0 K can be attributed to inhomogeneous broadening, Γ_{inh}, as a result of the nonrelaxed environmental heterogeneity around the excited guest molecules. Thus, the data in Fig. 2 indicate a structural correlation between the size of the lateral alkyl group of the PAMAs (which also plays a large role in determining their physical properties) and the magnitude of the inhomogeneous broadening at 0 K. The values of Γ_{inh} increase from 215 cm^{-1} for PCHMA to 350 cm^{-1} for PHDMA (Table 1). Except for PIBMA, the higher the T_g is the smaller is the broadening.

The arrows in Fig. 2 show the temperatures of the onsets of the polymer relaxation processes determined from emission spectra (17). The FWHM is insensitive to polymer relaxation processes at lower temperatures (T_γ = 120–150 K), γ-relaxation is attributed to rotations of the ester groups (1–5), but the curves show pronounced slope changes for processes involving larger segments (T_β = 220–270 K), β-relaxation involves the rotation of the ester side groups (1–5,17). Movements of the backbone chains (α-relaxation) in several PAMAs are available over wide temperature ranges. In general, β-relaxations (involving the side groups) and α-relaxations (involving the main chain) in acrylates are strongly coupled processes (2,50,51). Thus, the relaxation processes involving shorter polymer segments do not alter the cybotactic regions around the pyrene molecules sufficiently to produce discernible changes of the inhomogeneous broadening. The locations of the segments involved in γ-relaxations (Fig. 3) are probably far from the cybotactic regions where pyrene molecules reside, and, thus, the guest molecules do not sense changes in the dielectric properties of their sites during their singlet excited-state lifetimes.

To assess qualitatively the disturbing influence of placing the pyrene probe molecules within the PAMA matrixes, the changes in the FWHM and the hole free volumes were compared over the temperature ranges encompassing the glass/melting temperature transitions (*i.e.* where the greatest sensitivities were observed) (Fig. 4). As can be seen, the changes in the two parameters are remarkably similar in trend, indicating that the pyrene molecules are incorporated into the PAMAs without appreciable disturbance to the dynamic properties of their cybotactic layers. Although the conformations of the polymer chain segments immediately next to the pyrene molecules must be different in the absence of the guests, their presence does not alter significantly the ability of the segments to undergo dynamic changes. As the positron annihilation technique includes the sites of largest hole free volumes (whose mean values are smaller than the van der Waals volume of a pyrene molecule, 322 $Å^3$) (10,52), it is reasonable to assume that they are the predominant sites which become the cybotactic regions. Thus, we conclude

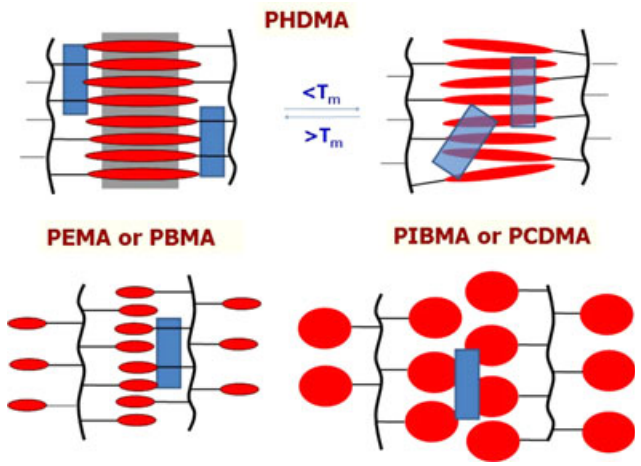

Figure 3. Cartoon representation of the possible locations of pyrene molecules (blue rectangles) in PAMA films. Side groups and polymer backbones are shown as red objects and curved lines, respectively. The gray area in the PHDMA below T_m is the crystalline region where guest molecules cannot enter. Regions of γ-relaxations are on side group segments farthest from the main chains.

that the changes detected in the FWHM of peak I reflect the properties of the neat PAMAs.

To estimate the contribution of the spectral homogeneous broadening, we assumed that Γ_{inh} is temperature independent in the range 20–100 K, and that Γ_{hom} can be given by the difference between the spectral broadening at a certain T, $\Gamma(T)$, and the value extrapolated to 0 K, $\Gamma(T = 0\ \text{K})$ (Table 1). In this regard, note that the temperature dependence in the lower temperature range ($T < 100$ K) is very similar in the five PAMAs (Fig. 5); the significant error limits in this region are larger than at higher temperatures because the differences being measured are very small.

The temperature dependence of the homogeneous linewidths at lower temperatures for molecules in some organic glasses may be described by a power law (Eq. 1) with a power coefficient, $\alpha = 1.3 \pm 0.1$, when spectral diffusion is the most important process (25,26,31–33,35). Thus, by fitting the experimental curves in Fig. 5, α(PCHMA) = 1.3 ± 0.2, α(PBMA) = 1.3 ± 0.3, α(PIBMA) = 1.2 ± 0.4, α(PHDMA) = 2.2 ± 0.7 and α(PEMA) = 0.8 ± 0.1 (Figure S2). Interestingly, all the values, except that for PEMA, are in the range expected for the temperature dependence of the spectral diffusion process. It has not been possible to understand why PEMA behaves differently with the data available.

Several reports indicate that no single temperature dependence is expected to describe spectral homogeneous broadening in all glassy materials (22,27–30,33,35). However, a general behavior might be described using reduced properties, $\frac{\Gamma(T)-\Gamma(T=0\,\text{K})}{\Gamma(T_g)-\Gamma(T=0\,\text{K})}$ and T/T_g or T/T_m (29). In Fig. 6, the reduced spectral broadening is plotted *versus* reduced temperature; T_g values are taken from Table 1. These curves can be divided roughly into three regions: 20–100 K (*i.e.* $0 < T/T_g < 0.35$), where no discernible relaxations occur and all curves overlap; $0.35 < T/T_g < 1$, where both γ- and β-relaxation processes operate and the curves are different for the PAMAs; in the range $1 < T/T_g < 1.4$ where all the curves change in a similar fashion. Thus, these PAMAs are not behaving as simple organic glasses. They are described better as dynamic environments undergoing polymer relaxation processes that produce additional contributions to the inhomogeneous broadening.

In summary, one may categorize these PAMAs into three groups: PHDMA (a semicyrstalline polymer near room temperature) induces greater inhomogeneous broadening and, thus, very

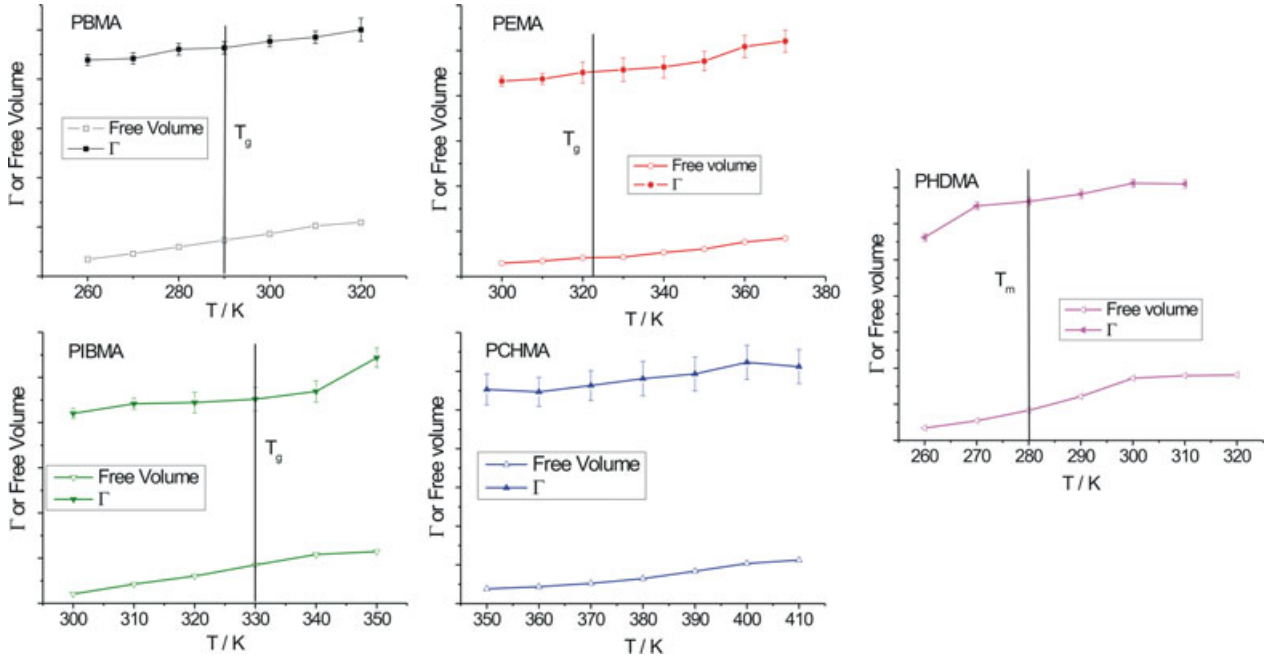

Figure 4. Comparison of hole free volumes (Å^3) and FWHM (Γ) values (cm^{-1}) in the PAMA films *versus* temperature in the ranges encompassing the glass or melting transition temperatures. The error bars are based upon the differences between the average values for two separate runs on two different samples.

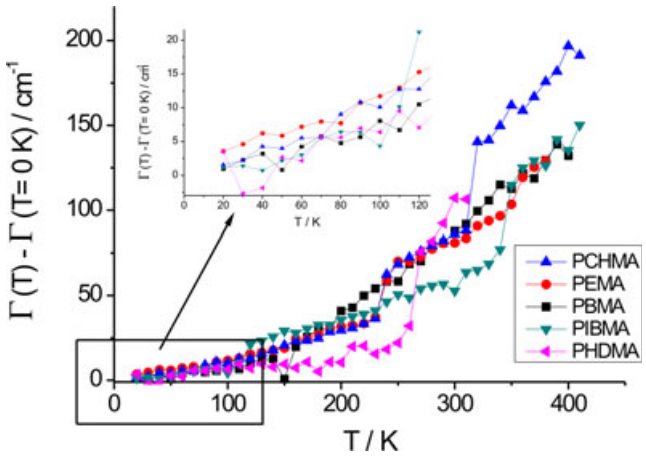

Figure 5. Differential spectral broadening for peak I of the pyrene emission in the PAMA matrixes. The inset depicts the temperature range 20–100 K used to simulate the temperature dependence of the FWHM using Eq. (1) (Figure S4).

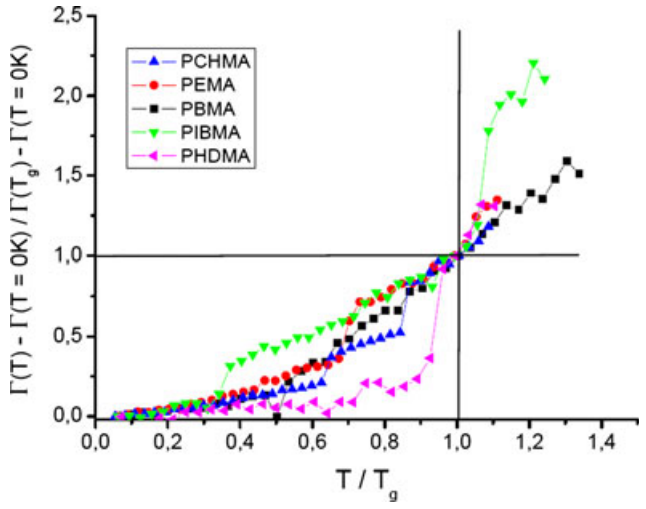

Figure 6. Reduced spectral broadening $\frac{\Gamma(T)-\Gamma(T=0\,\mathrm{K})}{\Gamma(T_g)-\Gamma(T=0\,\mathrm{K})}$ *versus* reduced temperature T/T_g or T/T_m as monitored by pyrene emissions in the PAMA films.

heterogeneous cybotactic environments for the pyrene molecules; in PEMA, PBMA and PCHMA the inhomogeneous broadening follows an inverse relationship with glass transition temperatures (the lower the T_g, the greater the Γ); PIBMA has a higher T_g and induces a greater heterogeneous cybotatic environment than does the isomeric PBMA due to the influence of the bulkier isobutyl groups on the regions near the main polymer chains. Also, the similarity between the temperature dependencies on spectral broadening and hole free volume indicates that the nature of the molecular probe or process being investigated may be very important in assessing the role of a polymer matrix; our previous studies, in which the diffusion of benzylic radicals was measured in the same PAMAs (13), showed no obvious correlation with hole free volume.

In addition to the changes in the spectral broadening, a small red spectral shift was observed for peak I in the pyrene emissions in the five PAMAs. These shifts are plotted as the difference between the peak position at 0 K (obtained by extrapolation) and at temperatures T (see Figure S5). The shifts are a consequence of the redistribution of the exciton energies by electron–phonon interactions, activating lower energy acoustical or optical phonons within the host matrixes (31–33,38–40). The best fits of the experimental data to Eq. (2) are also shown as continuous curves in Figure S5. The fits are quite good in the higher temperature regimes (where some relaxation processes are occurring and coupling between the pyrene emissions and the chains of the cybotactic regions are expected to be important). Using the best fits, the a parameters, corresponding to the strength of the electron–phonon interactions, and the phonon temperatures θ, have been calculated (Table 2). Values of a are between 219 cm^{-1} (27 meV) in PCHMA and are much lower (and indicating less efficient coupling), 43.54 cm^{-1} (5.4 meV), in PHDMA. These energies are in the range of torsional barriers of organic molecules in polymer matrixes and of macromolecular conformational changes of conjugated polymers, and oligomers and some biological molecules (33,38,53–55). Values of θ are between 481 K for PCHMA and 212 K for PHDMA, and the decrease follows the same trends as the glass transition temperatures, the FWHMs, and the a parameters. Furthermore, the range of the θ values is similar to that observed when the mechanism for the electron–phonon coupling involves optical transversal modes (*i.e.* normal modes associated with torsional vibrations), as found from conjugated oligomers, and some organic guest molecules in polymers (24,54,55). Thus, again there is a structural correlation between this type of coupling and the macromolecular physical properties of the PAMA matrixes.

Table 2. Parameters for electron–phonon interactions (a), phonon temperatures (θ) and the coefficients of quality of the fits (R) to Eq. (2) (Figure S5). See text for details.

PAMA	a/(cm^{-1})/(meV)	θ/K	R
PCHMA	219/27	481	0.9929
PEMA	186/23	448	0.9927
PIBMA	127/15.8	365	0.9925
PBMA	138/17.1	386	0.9924
PHDMA	43.5/5.4	212	0.9545

It has been proposed that the phonon temperature θ induces a noticeable excitation of the thermal vibrations at $T_{exp} \sim \theta/3$, which gave values of T_{exp} between 160 K for PCHMA to 120 K for PHDMA using data from Table 2. This is the temperature range observed for the onset of the γ-relaxation process of these polymers, which is attributed to motions of small segments of the lateral groups. The photophysical consequence of these thermal-activated motions is the onset of the decrease in the fluorescence intensity or in other words, the temperature range where the nonradiative pathways are thermally activated as showed in Ref. (17).

Also, in an earlier report (17), we suggested that the temperature dependence of the vibronic intensity ratio for the highest and third highest energy emission bands from pyrene, I_1/I_3, might be related to electron–phonon coupling. That suggestion has now been verified by the treatment presented here of the temperature dependence of the peak I position. As the transversal optical modes are activated, the electron–phonon coupling and, thus, the I_1/I_3 ratio changes markedly; peak I (*i.e.* band 1) intensity decreases relative to that of band 3. Franck–Condon analysis of the vibronic bands can be performed using the Huang–Rhys electron–phonon model (43). This model might be useful to

explain changes in the vibronic intensity as a function of the temperature (56) as observed and described in Ref. (17). However, this simulation might be complicated for pyrene (studies are in progress) as in addition to the Franck–Condon effect, Hezberg–Teller effect is also involved in the vibronic structure of the pyrene emission bands (57).

CONCLUSIONS

Possible relationships between line broadening of the fluorescence from pyrene guest molecules and both the order and hole free volumes of the matrixes of the PAMAs over a very broad temperature range have been demonstrated using a power law dependence to relate spectral broadening and phonon coupling. Additional spectral features, the peak positions and the full width at half maximum of the 0–0 emission band, have been examined carefully to obtain information about the temperature dependence of inhomogeneous and homogeneous line broadening on different distributions of the cybotactic sites afforded to the pyrene guests and their host–guest interactions, and on the efficiency of electron–phonon coupling. The magnitude of the electron–phonon interactions is related to transversal optical modes and is correlated with the polymer structure: it is stronger for PAMAs with higher glass transition temperatures. Surprisingly, given our previous results with a diffusion-based probe system using the same PAMAs, (13) the FWHM changes correlate very well with hole free volume, at least over a temperature range which includes the glass or melting transitions. From the results, it has been possible to devise a model for where the pyrene molecules reside preferentially within the inhomogeneous matrixes of the polymer hosts. Perhaps more importantly, the approach presented here should be amenable to analyzing the interactions between a large range of guest molecules in many different types of neat polymer matrixes.

Acknowledgements—TDZA acknowledges FAPESP, CNPq, the National Institute of Organic Electronics (INEO) (MCT/CNPq/FAPESP) and UNICAMP/FAEPEX for financial support and fellowships. SA and RGW thank the U. S. National Science Foundation for its support of this research through grants CHE-1147353 and CHE-0911089. SJP and AJH acknowledge the Australian Research Council and the CSIRO Office of the Chief Executive Science Team for funding.

SUPPORTING INFORMATION

Additional Supporting Information may be found in the online version of this article:

Figure S1. Photoluminescence spectra of pyrene in four PAMA films at several temperatures from 20 to 410 K.

Figure S2. Comparison of analyzed data for pyrene fluorescence in two PBMA films, including the wavenumber of peak I, FWHM for peak I (Γ in cm^{-1}), $\Gamma(T) - \Gamma(T = 0\ K)$ and $\frac{\Gamma(T)-\Gamma(T=0\,K)}{\Gamma(T_g)-\Gamma(T=0\,K)}$ obtained by fitting the emission spectra using Gaussian functions.

Figure S3. Comparison of analyzed data for pyrene fluorescence in two PCHMA films, including the wavenumber of peak I, FWHM for peak I (Γ in cm^{-1}), $\Gamma(T) - \Gamma(T = 0\ K)$ and $\frac{\Gamma(T)-\Gamma(T=0\,K)}{\Gamma(T_g)-\Gamma(T=0\,K)}$ obtained by fitting the emission spectra using Gaussian functions.

Figure S4. FWHM of peak I of the photoluminescence using spectral deconvolution with Gaussian functions of pyrene in five PAMA films at several temperatures. The continuous curve is the simulation using Eq. (1).

Figure S5. Temperature dependence of the redshift of peak I of the pyrene emission in PAMA matrixes. The continuous curves are best fits to Eq. (2).

REFERENCES

1. Hempel, E., H. Huth and M. Beiner (2003) Interrelation between side chain crystallization and dynamic glass transitions in higher poly(n-alkyl methacrylates). *Thermochim. Acta* **403**, 105–114.
2. Wind, M., R. Graft, S. Renker and H. W. Spiess (2005) Structural reasons for restricted backbone motion in poly(*n*-alkyl methacrylates): Degree of polymerization, tacticity and side-chain length. *Macromol. Chem. Phys.* **206**, 142–156.
3. Becker-Guedes, F., E. R. deAzevedo, T. J. Bonagamba and K. Schmidt-Rohr (2004) Solid-state exchange NMR characterization of segmental dynamics in glassy poly(alkyl methacrylate). *Appl. Magn. Reson.* **27**, 383–400.
4. McCrum, N. G., B. E. Read and G. Williams (1976) *Anelastic and Dielectric Effects in Polymer Solids*. Wiley, London.
5. Beiner, M., O. Kabisch, S. Reichl and H. Huth (2002) Structural and dynamic nanoheterogeneities in higher poly(alkyl methacrylate)s. *J. Non-Cryst. Solids* **307**, 658–666.
6. Valeur, B. (2002) *Molecular Fluorescence Principles and Applications*, pp. 34–70. WILEY-VCH, Weinheim.
7. Zaitsev, V. B., G. S. Plotnikov and A. M. Saletskii (2009) Optical methods in studies of structural transformation in thin organic films. *Phys. Bull.* **64**, 287–290.
8. Tomin, I. and K. Hubisz (2006) Inhomogeneous spectral broadening and the decay kinetics of the luminescence spectra of prodan. *Opt. Spectrosc.* **101**, 98–104.
9. Luo, C., T. D. Z. Atvars, P. Meakin, A. J. Hill and R. G. Weiss (2003) Determination of initial and long-term microstructure changes in ultrahigh molecular weight polyethylene induced by drawing neat and pyrenyl modified films. *J. Am. Chem. Soc.* **125**, 11879–11892.
10. Prado, E. A., S. B. Yamaki, T. D. Z. Atvars, O. E. Zimerman and R. G. Weiss (2000) Static and dynamic fluorescence of pyrene as probes of site polarity and morphology in ethylene-co-(vinyl acetate) (EVA) films. *J. Phys. Chem. B* **104**, 5905–5914.
11. Barja, B. C., C. Chesta, T. D. Z. Atvars and P. F. Aramendia (2005) Relaxations in poly(vinyl alcohol) and in poly(vinyl acetate) detected by fluorescence emission of 4-aminophthalimide and Prodan. *J. Phys. Chem. B* **109**, 16180–16187.
12. Baldi, L. D. C., E. T. Iamazaki and T. D. Z. Atvars (2008) Evaluation of the polarity of polyamide surfaces using the fluorescence emission of pyrene. *Dyes Pigm.* **76**, 669–676.
13. Abraham, S., I. Ghosh, W. M. Nau, C. Chesta, S. J. Pas, A. J. Hill and R. G. Weiss (2012) In-cage and out-of-cage combinations of benzylic radical pairs in the glassy and melted states of poly(alkyl methacrylate)s. *Photochem. Photobiol. Sci.* **11**, 914–924.
14. Chen, Y.-Z. and R. G. Weiss (2009) Photoreactions of substituted o-cresyl acylates in cyclohexane and in polyethylene films. The influences of intra- and inter-molecular "crowding' effects". *Photochem. Photobiol. Sci.* **8**, 916–925.
15. Abraham, S. and R. G. Weiss (2011) Photochemical and photophysical studies in bulk polymers and supramolecular effects in photochemistry. In *Supramolecular Effects in Photochemistry* (Edited by V. Ramamurthy and Y. Inoue), pp. 443–516. Wiley, New York.
16. Chesta, C. A. and R. G. Weiss (2010) Dynamics of radical pair processes in bulk polymers. In *Carbon-Centered Radicals and Radical Ions* (Edited by M. D. E. Forbes), pp 281–324. Wiley, Hoboken, NJ.
17. Abraham, S., T. D. Z. Atvars and R. G. Weiss (2010) Effects of temperature and alkyl groups of poly(alkyl methacrylate)s on inter- and intra-molecular interactions of excited singlet states of pyrenyl guest molecules. *J. Phys. Chem. B* **114**, 12221–12233.
18. Duda, J. L. and J. M. Zielinski (1996) Free-volume theory. In *Diffusion in Polymers* (Edited by P. Neogi). Marcel Decker, Inc., New York.

19. Bandzuch, P., J. Kristiak, O. Sausa and J. Zrubcova (2000) Direct computation of the free volume fraction in amorphous polymers from positron lifetime measurements. *Phys. Rev. B* **61**, 8784–8792.
20. Zimerman, O. E. and R. G. Weiss (1998) Static and dynamic fluorescence from α,ω-di(1-pyrenyl)alkanes in polyethylene films. Control of probe conformations and information about microstructure of the media. *J. Phys. Chem. A* **102**, 5364–5374.
21. Martins, T. D., S. B. Yamaki, E. A. Prado and T. D. Z. Atvars (2003) Broadening of the fluorescence spectra of hydrocarbons in ethylene-vinyl acetate copolymers and the dynamics of the glass transition. *J. Photochem. Photobiol. A Chem.* **156**, 91–103.
22. Brown, R., S. Lacombe and H. Cardy (2003) Interpretation of spectral broadening and clustering of a pyrene derivative adsorbed in silica gels. *Microporous Mesoporous Mater.* **59**, 93–103.
23. Leontidis, E., U. W. Suter, J. M. Schutz, H.-P. Liithi, A. Rem and U. P. Wild (1995) The mechanism of spectral shift and inhomogeneous broadening of an aromatic chromophore in a polymer glass. *J. Am. Chem. Soc.* **177**, 7493–7507.
24. Renge, I. (2006) Influence of temperature and pressure on shape and shift of impurity optical bands in polymer glasses. *J. Phys. Chem. A* **110**, 3533–3545.
25. Schmidt, Th., J. Baak, D. A. van de Straat, H. B. Brom and S. Völker (1993) Temperature dependence of optical linewidths and specific heat of rare-earth-doped silicate glasses. *Phys. Rev. Lett.* **71**, 3031–3034.
26. Mcfarlane, R. M. and R. M. Shelby (1987) Homogeneous line broadening of optical transitions of ions and molecules in glasses. *J. Lumin.* **36**, 179–207.
27. Meyers, A. B. (1998) Molecular electronic broadening in liquids and glasses. *Ann. Rev. Phys. Chem.* **49**, 267–299.
28. Leontidis, E., H. Heinz, K. Palewska, E.-U. Wallenborn and U. W. Suter (2001) Normal and defective perylene substitution sites in alkane crystals. *J. Chem. Phys.* **114**, 3224–3235.
29. Tormakoff, A. and M. D. Fayer (1995) Homogeneous vibrational dynamics and inhomogeneous broadening in glass-forming liquids: infrared photon echo experiments from room temperature to 10 K. *J. Chem. Phys.* **103**, 2810–2826.
30. Berg, M., C. A. Walsh, L. R. Narasimhan, K. A. Littau and M. D. Fayer (1988) Dynamics in low temperature glasses: Theory and experiments on optical dephasing, spectral diffusion, and hydrogen tunneling. *J. Chem. Phys.* **88**, 1564–1587.
31. Stein, S. and M. D. Fayer (1991) Nanosecond timescale optical inhomogeneous broadening of dye molecules in liquids at and near room temperature. *Chem. Phys. Lett.* **176**, 159–166.
32. Nemkovich, N. A., A. N. Rubinov and V. T. Tomim (1991) Inhomogeneous broadening of dye molecules in solutions. In *Topics in Fluorescence Spectroscopy*, Vol. II (Edited by J. R. Lackowicz), pp. 367. Plenum Press, New York.
33. Balzer, F., A. Pogantsch and H.-G. Rubaha (2009) Temperature dependence analysis of three classes of fluorescence spectra from p-6P nanofiberfilmes. *J. Luminescence* **129**, 784–789.
34. den Hartog, F. T. H., C. van Papendrecht, R. J. Silbey and S. Völker (1999) Spectral diffusion by energy transfer in doped organic glasses: Delay-time dependence of spectral holes. *J. Chem. Phys.* **110**, 1010–1016.
35. Shelby, R. M. (1983) Measurement of optical homogeneous linewidths in a glass with picosecond accumulated photon echoes. *Opt. Lett.* **8**, 88–90.
36. Koedijk, J. M. A., R. Wannemacher, R. J. Silbey and S. Völker (1994) Spectral diffusion in organic glasses: Time dependence of spectral holes. *J. Phys. Chem.* **100**, 19945–19953.
37. Peterman, E. J. G., T. Pullrits, R. van Grondelle and H. van Amerongen (1997) Electron-phonon coupling and vibronic fine structure of light-harvesting complex II of green plants: Temperature dependent absorption and high-resolution fluorescence spectroscopy. *J. Phys. Chem. B* **101**, 4448–4457.
38. Renge, I. (2003) Thermal effects on zero-phonon holes in the optical spectra molecular probes in polymer glasses. *Phys. Rev. B* **68**, 064205.
39. Guha, S., J. D. Rice, Y. T. Yau, C. M. Martin, M. Chandrasekhar, H. R. Chandrasekhar, R. Guentner, P. Scanduicci de Fretias and U. Scherf (2003) Temperature–dependent photoluminescence of organic semiconductors with varying backbone conformation. *Phys. Rev. B* **67**, 125204.
40. Vina, L., S. Logothetidis and M. Cardona (1984) Temperature dependence of the dielectric function of germanium. *Phys. Rev. B* **30**, 1979–1991.
41. Bassler, H. and B. Schweitzer (1999) Site-selective fluorescence spectroscopy of conjugated polymers and oligomers. *Acc. Chem. Res.* **32**, 173–182.
42. Schlichter, J. and J. Friedrich (2001) Glasses and proteins: Similarities and differences in their spectral diffusion dynamics. *J. Chem. Phys.* **114**, 8718–8721.
43. Huang, K. and A. Rhys (1950) Theory of light absorption and nonradiative transitions in F-centres. *Proc. R. Soc. Lond. A* **204**, 406–423.
44. Zipper, M. D. and A. J. Hill (1994) The application of positron-annihilation lifetime spectroscopy to the study of glassy and partially crystalline materials. *Mater. Forum* **18**, 215–233.
45. Pascual-Izarra, C., A. W. Dong, S. J. Pas, A. J. Hill, B. J. Boyd and C. J. Drummond (2009) Advanced fitting algorithms for analyzing positron annihilation lifetime spectra. *Nucl. Instrum. Methods Phys. Res., Sect. A* **603**, 456–466.
46. Cui, C., J. Naciri, Z. He, R. M. Jenkins, L. Lu, V. Ramesh, G. S. Hammond and R. G. Weiss (1993) Photochemical and photophysical approaches to the characterization of the shapes, free volumes and accessibilities of guest sites in low-density polyethylene films. *Quim. Nova* **16**, 578–585.
47. Gu, W., A. J. Hill, X. Wang, C. Cui and R. G. Weiss (2000) Photorearrangements of five 1- and 2-naphthyl acylates in three unstretched and stretched polyethylene films. Does reaction selectivity correlate with free volumes measured by positron annihilation lifetime spectroscopy?. *Macromolecules* **33**, 7801–7811.
48. Birks, J. B. (1970) *Photophysics of Aromatic Molecules*, 118 pp. Wiley, London.
49. Kansy, J. (1996) Microcomputer program for analysis of positron annihilation lifetime spectra. *Nucl. Instrum. Methods Phys. Res. A* **374**, 235–244.
50. Ngai, K. L., T. R. Gopalakrishnan and M. Beiner (2006) Relaxation in poly(alkyl methacrylate)s: Change of intermolecular coupling with molecular structure, tacticity, molecular weight, copolymerization, crosslinking, and nanoconfinement. *Polymer* **47**, 7222–7230.
51. Fytas, G. (1989) Relaxation processes in amorphous poly(cyclohexy1 methacrylate) in the rubbery and glassy state studied by photon correlation spectroscopy. *Macromolecules* **22**, 211–215.
52. Camerman, A. and J. Trotter (1965) The crystal and molecular structure of pyrene. *Acta Cryst.* **18**, 636–643.
53. Vettegren, V. I., A. I. Slutsker and V. B. Kulik (2009) Stresses induced in polymer crystals by the atomic–molecular internal dynamics. *Phys. Solid State* **51**, 212–220.
54. O'Neil, L and H. J. Byrne (2005) Structure-property relationships for electron-vibrational coupling in conjugated oligomeric systems. *J. Phys. Chem. B* **109**, 12685–12690.
55. Gierschner, J., H.-G. Mack, L. Lüer and D. Oelrug (2002) Fluorescence and absorption spectra of oligophenylenevnylenes: Vibronic coupling, band shapes and solvatochromism. *J. Chem. Phys.* **116**, 8596–8609.
56. Hagler, T. W., K. Pakbaz, K. F. Voss and A. Heeger (1991) Enhanced order and electronic delocalization in conjugated polymers oriented by gel processing polethylene. *Phys. Rev. B* **44**, 8652–8666.
57. Karpovich, D. S. and G. J. Blanchard (1995) Relating the polarity-dependent fluorescence response of pyrene to vibronic coupling. Achieving a fundamental understanding of the py polarity scale. *J. Phys. Chem.* **99**, 3951–3958.